Chapter:4

Reduction of Leakage Current of Proposed L_nC_{2n-2} Network Based MOHC and Performance Analysis

4.1. Introduction

As previously discussed, the neutral of the AC terminal is grounded, and for safety reasons, the negative terminal of the PV panel is also grounded. Due to the large conductive surface of the PV panel, a parasitic capacitance naturally forms between the panel and the ground. Additionally, to effectively transfer power from the PV system to AC utilities or the grid, a power electronic interface is typically required. However, the high switching frequency of the power converter induces a rapid voltage change (dv/dt) across this parasitic capacitance, leading to the circulation of leakage current. This unwanted current not only results in power losses but also introduces electromagnetic interference (EMI) into the system, potentially affecting its overall performance.

In this chapter, how the proposed topology effectively mitigates leakage current and enhances system efficiency is explored. Furthermore, the proposed converter with existing topologies is discussed, highlighting its advantages. A detailed performance analysis is also presented to evaluate its effectiveness. Finally, experimental results are provided to validate the proposed concept and demonstrate its practical feasibility.

4.2. Minimisation of Leakage Current

Solar PV panels have a large conducting surface area, which leads to the formation of a parasitic capacitance (C_{PV}) between the panel and the ground. As a result, electrical charges accumulate on the surface of the PV panel. This buildup of charges can become hazardous—if a person comes into contact with the panel, the stored charges may discharge through their body, posing a serious safety risk. To mitigate this danger, PV

panels are typically grounded so that any accumulated charges can safely dissipate into the ground.

In order to harness power from PV panels, a power electronic converter is essential. However, the high-frequency switching operation of the converter induces a rapid voltage change (dV/dt) across the parasitic capacitance (C_{PV}). Since most electrical loads, utilities, and grids are AC-based—and their AC terminals are grounded for safety—this dV/dt stress gives rise to leakage currents. These leakage currents not only result in power losses but also cause electromagnetic interference (EMI) and additional safety concerns.

One common solution to mitigate leakage currents is to introduce a transformer between the PV panel and the grid. Transformers provide galvanic isolation, effectively eliminating leakage currents. However, transformers are costly and introduce their own

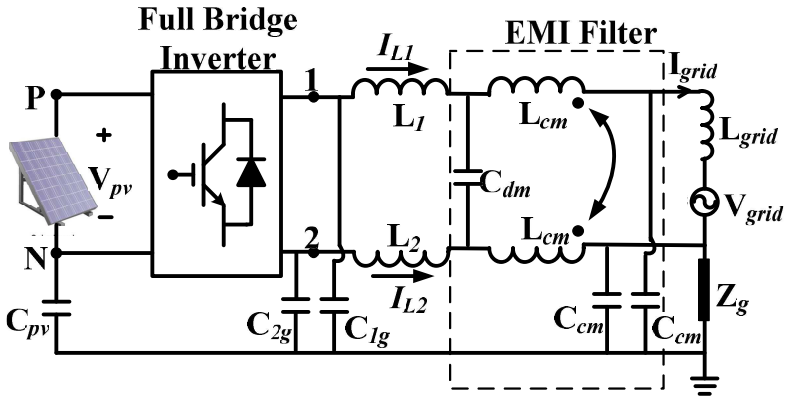

(a)

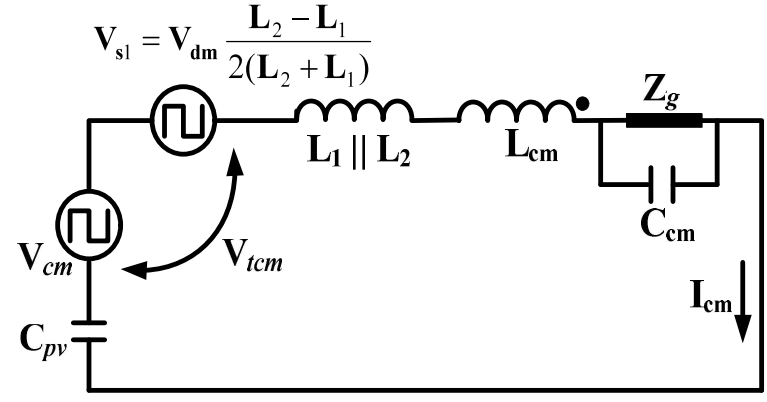

(b)

Fig. 4.1. Equivalent model for common-mode voltage and current: (a) Single phase full bridge neutral grounded inverter with parasitic elements (b) Final Thevenin equivalent for common mode voltage and current.

losses, making the system less efficient. This has driven the preference for transformerless systems in PV applications.

While many transformerless solutions have been proposed by researchers, most of these are only suitable for PV-to-AC systems. Some efforts have been made to develop transformerless solutions for multi-output hybrid converter (MOHC) systems, but these often fall short of delivering the standard DC and AC voltage ratings required for practical applications.

The PV panel and the grounded structure together form a parasitic capacitance, denoted as C_{PV}. This capacitance typically falls within the range of 50 to 150 nF per kilowatt, depending on several factors, such as the local climate, the grounding techniques used, and the manufacturing process of the PV panel.

To analysze the leakage current issue lets consider the case of a single-phase full-bridge neutral-grounded inverter, several electrical components come into play when analyzing the system's behavior. These include the electromagnetic interference (EMI) filter, the grid inductance (L_{grid}), the grounding impedance (Z_g), and two filter inductors, L_{f1} and L_{f2} — all illustrated in Fig. 4.1(a). Additionally, the Thevenin equivalent voltage across C_{PV} is depicted in Fig. 4.2(b).

Since the inverter employs a high-frequency pulse-width modulation (PWM) technique, it generates significant voltage stress across C_{PV} in terms of the rate of voltage change over time, often expressed as (dv/dt). This high-frequency switching gives rise to the formation of two distinct types of voltages: total common-mode voltage (V_{tcm}) and differential-mode voltage (V_{dm}).

TABLE 4.1

COMPLETE SWITCHING STATES OF THE PROPOSED CONVERTER

Modes	S_t	S_1	S_2	S_3	S_4	V_{1N}	V_{2N}	V_{cm}	V_{dm}
S_t (V_{ac}>0)	ON	OFF	ON	OFF	OFF	0	0	0	0
Zero (V_{ac}>0)	OFF	OFF	ON	OFF	OFF	0	0	0	0
Power (V_{ac}>0)	OFF	ON	ON	OFF	OFF	V_{dc}	0	$V_{dc}/2$	V_{dc}
S_t (V_{ac}<0)	ON	OFF	OFF	OFF	ON	0	0	0	0
Zero (V_{ac}<0)	OFF	OFF	OFF	OFF	ON	0	0	0	0
Power (V_{ac}<0)	OFF	OFF	OFF	ON	ON	0	V_{dc}	$V_{dc}/2$	$-V_{dc}$

TABLE 4.2

ANALYSIS OF TOTAL COMMON MODE VOLTAGE

Modes	V_{cm}	V_{dm}	V_{s1}	V_{tcm}
S_t (V_{ac}>0)	0	0	0	0
Zero (V_{ac}>0)	0	0	0	0
Power (V_{ac}>0)	$V_{dc}/2$	V_{dc}	$-V_{dc}/2$	0
S_t (V_{ac}<0)	0	0	0	0
Zero (V_{ac}<0)	0	0	0	0
Power (V_{ac}<0)	$V_{dc}/2$	$-V_{dc}$	$-V_{dc}/2$	0

The output voltages at the converter's ports 1 and 2, measured with respect to the reference port N, can be mathematically described as follows:

$$V_{cm} = \frac{V_{1N}+V_{2N}}{2} \tag{4.1}$$

$$V_{dm} = V_{1N} - V_{2N} \tag{4.2}$$

$$V_{1N} = V_{cm} + \frac{V_{dm}}{2} \tag{4.3}$$

$$V_{2N} = V_{cm} - \frac{V_{dm}}{2} \tag{4.4}$$

The Thevenin equivalent or the total common mode voltage across C_{PV} can be represented as follows:

$$V_{tcm} = V_{cm} + V_{s1} \tag{4.5}$$

$$V_{s1} = V_{dm}\frac{L_2-L_1}{2(L_2+L_1)} \tag{4.6}$$

For various configurations of filter inductors, the expression for V_{s1} can be given as:

$$V_{s1} = \begin{cases} 0 & L_{f1} = L_{f2} = \frac{L}{2} \\ -\frac{V_{dm}}{2} & L_{f1} = \frac{L}{2} \ \& \ L_{f2} = 0 \\ \frac{V_{dm}}{2} & L_{f1} = 0 \ \& \ L_{f2} = \frac{L}{2} \end{cases} \tag{4.7}$$

To minimize the leakage current, it is necessary to keep V_{tcm} (common-mode voltage) at a minimum or constant level. By selecting an appropriate configuration of the filter inductors and solving eq 4.7, it is possible to achieve a V_{tcm} value of zero.

The complete switching pattern, along with the corresponding values of common-mode voltage (V_{cm}) and differential-mode voltage (V_{dm}) for the proposed hybrid converter, is systematically presented in Table 4.1. This table outlines these values for different operating states, including the zero state, power state, and shoot-through state.

Building upon the data in Table 4.1, Table 4.2 is formulated to provide insights into the total common-mode voltage (V_{tcm}) across all operational states of the proposed hybrid converter. A key observation from Table 4.2 is that V_{tcm} remains constant and equals zero within the high-frequency (HF) leakage current model. This characteristic plays a crucial role in minimizing leakage current, reinforcing the effectiveness of the proposed transformerless hybrid converter in mitigating leakage-related issues.

4.3. Comparative Analysis

A comparison of various Multi-Output Hybrid Converter (MOHC) topologies is presented in Table 4.3. Among these, the topology described in [11] stands out for using the least number of switches and passive components. However, this simplicity comes at the cost of significantly high leakage current, which limits its practical application.

The topology proposed in [46] introduces a multi-level, multi-output hybrid converter that incorporates 8 switches and 7 passive components. While this design offers increased versatility, it fails to address the issue of leakage current, which remains a critical concern in transformerless systems.

Similarly, the topology described in [55] uses 6 switches and 5 passive components, striking a balance between component count and performance. In contrast, the topology

TABLE 4.3

COMPARATIVE ANALYSIS OF PROPOSED TOPOLOGY WITH EXISTING MOHC'S

Parameters	**[11]**	**[46]**	**[55]**	**[121]**	**Proposed Topology**
Controlled Switches	4	8	6	8	5
Passive Components	5	7	5	5	8
DC Gain	$\frac{1}{1-d}$	$\frac{1}{1-d}$	$\frac{1}{1-d}$	$\frac{1}{1-d}$	$\frac{1}{1-2d}$
Peak AC Voltage	$\frac{m_i V_{PV}}{1-d}$	$\frac{2m_i V_{PV}}{1-d}$	$\frac{m_i V_{PV}}{1-d}$	$\frac{m_i V_{PV}}{1-d}$	$\frac{m_i V_{PV}}{1-2d}$
Range for m_i & d	0<d<1 0<m_i<(1-d)	0<d<1 0<m_i<(1-d)	0<d<1 0<m_i<(1-d)	0<d<1 0<m_i<(1-d)	0<d<0.5 0<m_i<(1-d)
Leakage current	High	High	Low	Low	Low
Power Density	Low	High	Moderate	Moderate	High
Efficiency	High	Low	Moderate	Low	Moderate

in [121] employs 8 switches and 5 passive components and does achieve lower leakage current.

Despite their differences, these topologies share a common limitation in terms of voltage gain. With a DC voltage gain of $1/(1-d)$ and an AC voltage gain of $m_i/(1-d)$, they face challenges in achieving practical voltage levels. For instance, when an input voltage of 120V is applied to obtain typical output levels of 230V DC and 110V AC, the condition $d + m_i \leq 1$ is violated. This constraint creates a major barrier to reaching the desired voltage outputs, making these designs less viable for real-world applications.

When compared to the existing topologies presented in [11], [46], and [55], the proposed hybrid converter does exhibit slightly lower power density. However, it offers a significant advantage in terms of input voltage requirements. The proposed topology operates with a lower input voltage of 120V, whereas the topology described in [121] requires a higher input voltage of 180V to achieve standard output levels of 230V DC and 110V AC.

Moreover, if a lower input voltage of 120V were applied to the existing topologies [11], [46], [55] and [121], it would result in a violation of the $d + m_i \leq 1$ constraint. This breach prevents these topologies from reaching practical voltage levels, making them less feasible for real-world applications where lower input voltage operation is preferred.

Another important advantage of the proposed converter can be seen in Table 4.3: it achieves simultaneous multi-output functionality using only five controlled switches. This streamlined design significantly reduces control complexity compared to other existing topologies, making the proposed approach not only more efficient but also easier to implement and manage in practical systems.

4.4. Performance Analysis and Loss Distribution

To thoroughly assess the performance of the proposed Multi-Output Hybrid Converter (MOHC), it's essential to evaluate its behaviour under different loading and voltage conditions. This analysis helps determine the converter's efficiency, stability, and adaptability when faced with varying power demands and input voltage levels.

In addition to performance evaluation, understanding the converter's power losses and how those losses are distributed across its components is equally important. A detailed loss analysis provides insight into the sources of inefficiency, enabling opportunities for design improvements and optimization. These aspects are discussed in detail in the following sections.

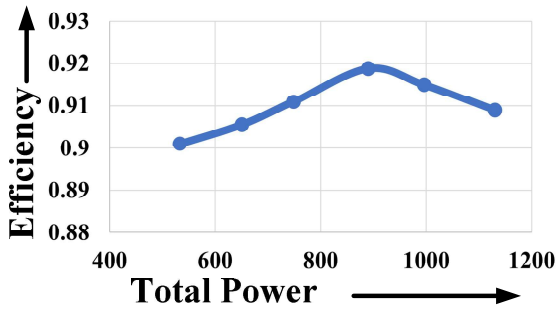

(a)

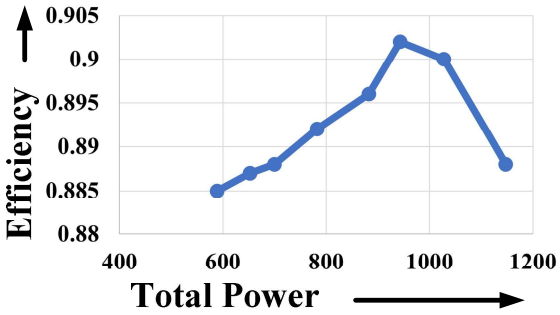

(b)

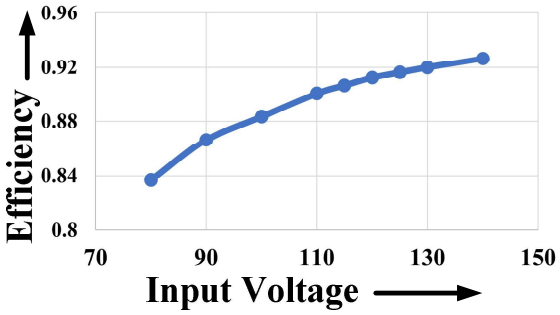

(c)

Fig. 4.2. Efficiency variation of the proposed converter at different loading conditions. (a) For DC load variation while keeping AC load constant. (b) For AC load variation while keeping DC load constant (c) For input voltage variation, keep DC and AC load constant.

4.4.1. Performance Analysis Under Varying Load and Input Voltage Conditions

The proposed converter stands out for its dual-output capability, delivering both DC and AC power from a single DC input source. To thoroughly evaluate its performance across different load conditions, two distinct energy profiles are considered. In the first profile, the DC load is varied while keeping the AC load constant, allowing an assessment of how changes in DC demand affect overall efficiency. In the second profile, the AC load is varied while the DC load remains fixed, providing insights into the converter's behaviour under fluctuating AC demand.

The efficiency of the converter is determined by comparing the total output power (DC + AC) with the input power. Input power is calculated by multiplying the measured input voltage (V_{PV}) with the measured input current (I_{PV}). Similarly, the DC output power is obtained from the product of the measured DC output voltage (V_{DC}) and DC output current (I_{DC}), while the AC output power is calculated by multiplying the measured AC output voltage (V_{AC}) with the AC output current (I_{AC}).

As illustrated in Fig. 4.2(a), the efficiency curve with a constant AC load and varying DC load reaches a peak efficiency of 92% at 900W. In Fig. 4.2(b), where the DC load remains fixed, and the AC load varies, the converter achieves a peak efficiency of 90.2% at 900W. Furthermore, Fig. 4.2(c) shows the efficiency curve as a function of input voltage variation.

It’s important to note that the converter’s efficiency can be further improved through careful optimization of the printed circuit board layout, selection of high-performance semiconductor devices, and the use of better-quality passive components. These enhancements could push the performance even closer to its theoretical limits, making the proposed system even more effective and reliable in practical applications.

4.4.2. Loss Distribution

The loss distribution of the proposed converter can be broadly divided into two parts, i.e., i) switching loss and ii) conduction loss, as can be seen in Fig. 4.3.

Switching Loss: Five IGBTs and four diodes are employed to switch the proposed converter, allowing it to deliver both AC and DC output simultaneously. To compute the total switching losses in the IGBTs (P_{total_S}) and diodes (P_{total_D}), refer to equation

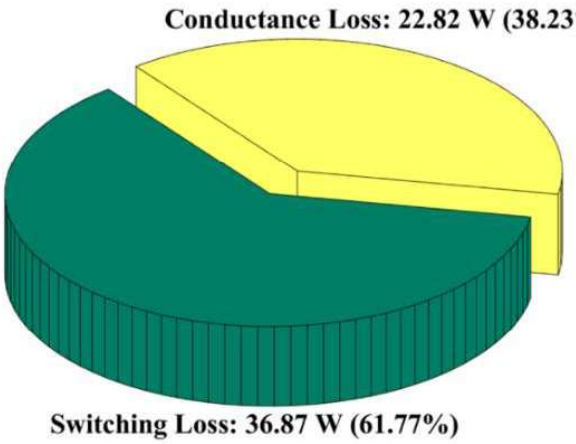

Fig. 4.3: Loss Distribution

(4.8). Furthermore, the total switching loss of the IGBTs (P_{total_S}) can be broadly divided into switching loss (P_{sw_S}) and conduction loss (P_{cond_S}), as shown in equation (4.9), where P_{sw_S} and P_{cond_S} are illustrated in (4.10) and (4.11) respectively. Similarly, the total switching loss of the diodes (P_{total_D}) can be categorized into switching loss (P_{sw_D}) and conduction loss (P_{cond_D}), as illustrated in equation (4.12) and P_{sw_D} and P_{cond_D} are illustrated in (4.13) and (4.14) respectively.

$$P_{total\_sw} = P_{total\_S} + P_{total\_D} \quad (4.8)$$

$$P_{total\_S} = P_{sw\_S} + P_{cond\_S} \quad (4.9)$$

Where,

$$P_{sw\_S} = f_s\,(E_{on} + E_{off})\frac{V_{DC}*I_{in}}{V_{ref}*I_{ref}} \quad (4.10)$$

$$P_{cond\_S} = (\,I_{in}V_{CE} + r_{CE}i^2).d \quad (4.11)$$

$$P_{total\_D} = P_{sw\_D} + P_{cond\_D} \quad (4.12)$$

$$P_{sw\_D} = f_s\,(E_{rec})\frac{V_{DC}*I_{in}}{V_{ref}*I_{ref}} \quad (4.13)$$

$$P_{cond\_D} = (\,I_{in}V_{CE} + r_{CE}i^2).(1\text{-}d) \quad (4.14)$$

According to the datasheet of the IKW75N60H3 IGBT used in the proposed converter and the datasheet of the RURG8060 diode, the total switching losses calculated for a 960 W output at a 10 kHz frequency using the above formulas are illustrated below. Since the fast recovery diode is used, thus P_{sw_D} is considered as zero.

$$P_{sw\_S} = 4.508\ \text{W} \quad (4.15)$$

$$P_{cond\_S} = 10.16\ \text{W} \quad (4.16)$$

$$P_{sw\_D} = 0\ \text{W} \quad (4.17)$$

$$P_{cond\_D} = 22.2\ \text{W} \quad (4.18)$$

Thus, $$P_{total\_S} = P_{sw\_S} + P_{cond\_S} + P_{sw\_D} + P_{cond\_D} \quad (4.19)$$

$$P_{total\_S} = 36.868 \text{ W} \quad (4.20)$$

Conduction loss: The conduction loss of the proposed converter is calculated in the inductors and capacitors of the L_2C_2 network, as well as in the AC and DC filters. The parasitic resistance of the inductor (R_L) is considered to be 0.04 ohms, and the equivalent series resistance (ESR) of the capacitor is considered to be 0.25 ohms. Additionally, the loss in the grid resistance is accounted for, with its value set at 1 ohm.

$$P_{L2C2} = 15.79 \text{ W} \quad (4.21)$$

$$P_{DCf} = 0.65 \text{ W} \quad (4.22)$$

$$P_{ACf} = 1.28 \text{ W} \quad (4.23)$$

$$P_{Rg} = 5.1 \text{ W} \quad (4.24)$$

Thus, $$P_{total\_C} = P_{L2C2} + P_{DCf} + P_{Acf} + P_{Rg} \quad (4.25)$$

$$P_{total\_C} = 22.82 \text{ W} \quad (4.26)$$

Thus, Total power loss within the proposed converter

$$P_{total} = P_{total\_sw} + P_{total\_C} \quad (4.27)$$

$$P_{total} = 59.688 \text{ W} \quad (4.28)$$

4.5. Experimental Verification

This chapter addresses the mitigation of leakage current in the Multi-Output Hybrid Converter (MOHC). While the proposed topology was developed and verified for multi-output operations in the previous chapter, the issue of leakage current — a critical consideration for PV to AC-connected systems — was not explored. Leakage current can lead to safety concerns and affect system performance, making its mitigation essential. Therefore, this chapter presents a detailed investigation and validation of the proposed leakage current mitigation approach under both off-grid and on-grid operating conditions.

4.5.1. Minimization of Leakage Current Under OFF-Grid Conditions

In Fig. 4.4(a), the leakage current profile of the proposed converter is presented in the OFF-Grid conditions, demonstrating impressively low stress on the parasitic capacitor (C_{PV}). The leakage current remains well below the acceptable safety threshold of 300mA, highlighting the converter's effective design in minimizing unwanted current paths. Alongside this, Fig. 4.4(a) also shows the output AC voltage and current,

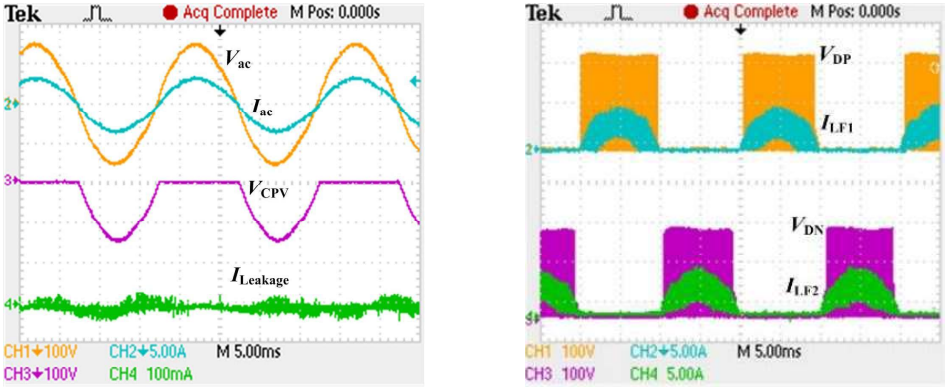

(a) (b)

Fig. 4.4. AC Characteristics and leakage current profile in OFF-Grid conditions (a) Leakage current profile. (b) Voltage stress across D_1 and D_2 along with AC inductors current.

measured at a steady 110V rms and 2A, respectively — indicating stable and reliable performance.

On the other hand, Fig. 4.4(b) provides insight into the voltage stress experienced by the diodes D_P and D_N in the AC section of the converter. It also captures the behaviour of the filter inductor currents, I_{LF1} and $I_{LF2,}$ offering a clear view of the current distribution and dynamic response within the filtering stage. Together, these waveforms illustrate the converter's efficient operation and well-managed component stresses.

4.5.2. Mitigation of Leakage Current Under ON-Grid Conditions

In Fig. 4.5(a), we can see the waveform of the grid voltage, which is a standard 110V AC supply. What's important here is that the voltage from the converter is perfectly

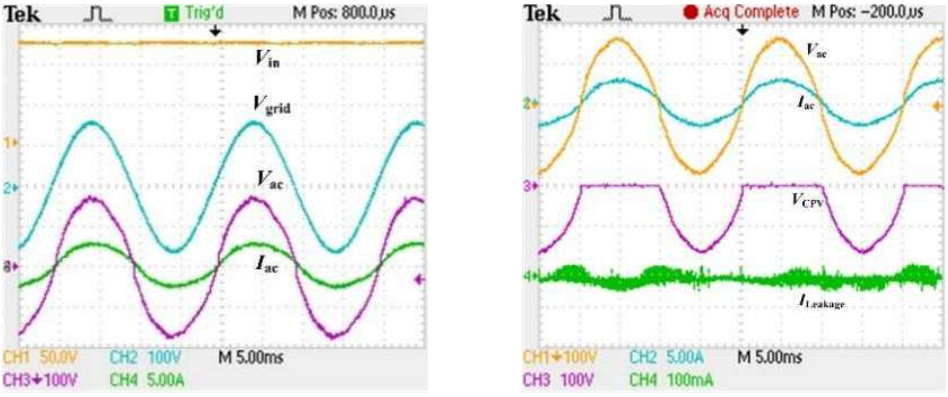

(a) (b)

Fig. 4.5. AC Characteristics, and Leakage current of L_2C_2-HC in ON-Grid operation (a) AC voltage and current with the PV input and grid voltage. (b) Leakage current profile.

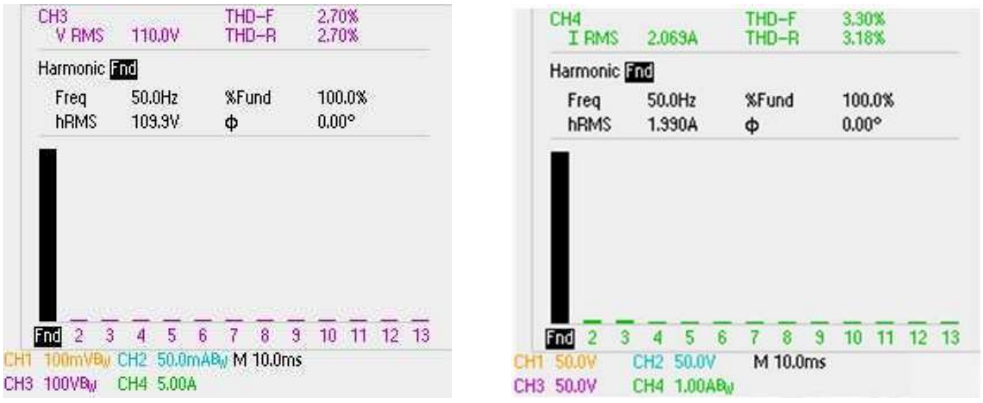

(a) (b)

Fig. 4.5. Total harmonic distortion (a) Grid Voltage. (b) Grid current.

synchronized with the grid voltage — they're in phase with each other. Additionally, the grid current injected into the grid is also shown, demonstrating the smooth and stable operation of the system.

On the other hand, Fig. 4.5(b) illustrates the behaviour of the leakage current. It's scaled at 100mA, making it easy to observe even small variations. The key takeaway here is that the leakage current stays well within the acceptable safety limits, ensuring safe and reliable system performance.

4.5.3. Total Harmonic Distortion

When a system operates in grid-connected mode, two critical performance factors come into play: Total Harmonic Distortion (THD) and leakage current. THD measures the quality of the voltage and current waveforms, while leakage current impacts safety and efficiency.

As discussed in the previous section, the system successfully minimizes leakage current in both On-Grid and Off-Grid modes, ensuring safe and stable operation. In addition to that, the THD levels of the AC grid voltage and the current fed into the grid are well-controlled. Specifically, Fig. 4.6(a) shows a voltage THD of 2.7%, while Fig. 4.6(b) displays a current THD of 3.3%. These values indicate that the system maintains good power quality, keeping harmonic distortion within acceptable limits.

4.6. Summary

This chapter focuses on the approach used to minimize leakage current, which is a crucial requirement for transformerless systems operating in both off-grid and on-grid configurations. Leakage current control is essential for ensuring system safety, efficiency, and compliance with operational standards.

One key highlight of this work is that, so far, none of the previously proposed transformerless Multi-Output Hybrid Converters (MOHC) have been validated under standard voltage ratings while maintaining minimized leakage current. In this context, the proposed MOHC stands out by addressing this gap effectively.

A detailed comparison of the proposed converter with existing MOHC topologies reveals its significant advantages. The proposed design uses a minimal number of switches, making it not only more efficient but also a cost-effective solution by reducing component count and overall system complexity.

The chapter also evaluates the performance of the proposed MOHC under varying load and input voltage conditions. An efficiency curve is plotted to illustrate the system's effectiveness across different operating scenarios. In addition, a thorough loss analysis is conducted, providing a detailed breakdown and calculation of power losses within the converter.

Finally, experimental results are presented to validate the concept of leakage current minimization. These results demonstrate the practical feasibility and performance of the proposed system.

While this chapter focuses on leakage current minimization and performance evaluation, however the control strategy of the proposed MOHC is not discussed here — that topic is covered in detail in the following chapter.